

# LGN-Net: Local-Global Normality Network for Video Anomaly Detection

Mengyang Zhao , Graduate Student Member, IEEE, Yang Liu , Graduate Student Member, IEEE, Jing Liu , Graduate Student Member, IEEE, Di Li  and Xinhua Zeng

**Abstract**—Video anomaly detection (VAD) has been intensively studied for years because of its potential applications in intelligent video systems. Existing unsupervised VAD methods tend to learn normality from training sets consisting of only normal videos and regard instances deviating from such normality as anomalies. However, they often consider only local or global normality. Some of them focus on learning local spatiotemporal representations from consecutive frames in video clips to enhance the representation for normal events. But powerful representation allows these methods to represent some anomalies and causes missed detections. In contrast, the other methods are devoted to memorizing global prototypical patterns of whole training videos to weaken the generalization for anomalies, which also restricts them to represent diverse normal patterns and causes false alarms. To this end, we propose a two-branch model, Local-Global Normality Network (LGN-Net), to learn local and global normality simultaneously. Specifically, one branch learns the evolution regularities of appearance and motion from consecutive frames as local normality utilizing a spatiotemporal prediction network, while the other branch memorizes prototype features of the whole videos as global normality by a memory module. LGN-Net achieves a balance of representing normal and abnormal instances by fusing local and global normality. The fused normality enables our model more generalized to various scenes compared to exploiting single normality. Experiments demonstrate the effectiveness and superior performance of our method. The code is available online: <https://github.com/Myzhao1999/LGN-Net>.

**Index Terms**—Video anomaly detection, spatiotemporal representation, memory network, normality learning.

## I. INTRODUCTION

VIDEO anomaly detection (VAD) refers to identify frames where abnormal events occur. It has been intensively studied because of its potential to be used in intelligent surveillance video systems [1]–[6]. However, it is still a challenging task due to the unbounded and rare nature of anomalies [7]. In other words, it is expensive or impossible to collect all types of abnormal events. In a real application scenario, models will be challenged by a variety of abnormal events that have never occurred before. Therefore, it is impractical to address VAD task using a binary classification approach.

This work was supported in part by the Science and Technology Commission of Shanghai Municipality Research Fund (Grant No. 21JC1405300), in part by the National Key Research and Development Program of China (Grant No. 2018YFC0831102) and in part by the Shanghai Key Research Lab. of NSAI. (Corresponding author: Xinhua Zeng.)

Mengyang Zhao, Yang Liu, Jing Liu and Xinhua Zeng are with the Academy for Engineering & Technology, Fudan University, Shanghai 200433, China (e-mails: {myzhao20, yang\_liu20, jingliu19, zengxh}@fudan.edu.cn).

Di Li is with the College of Information Engineering, Henan University of Science and Technology, Luoyang 471000, China (e-mail: lidistu.haust.edu.cn).

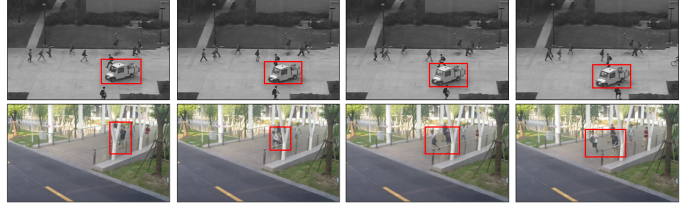


Fig. 1. Two abnormal samples from UCSD ped2 [20] (upper) and ShanghaiTech [21] (lower) datasets. The locations of abnormal events are marked by red bounding boxes.

To solve this issue, an intuitive idea is to consider anomalies as unexpected instances or the instances deviating from normal patterns. For example, a vehicle appears on a sidewalk and a robbery occurs on campus as shown in Fig. 1. These events are distinct from the normal behaviors or are unexpected in that scene. Based on this perspective, many unsupervised methods have been proposed with remarkable achievements in recent years [7]–[14]. These methods typically perform a proxy task (reconstruction or prediction task) to learn the normality from training sets consisting of only normal videos. In testing phase, abnormal instances will be distinguished as they usually receive high reconstruction or prediction errors. Prediction-based methods [15]–[17] typically take frame sequences consisting of several consecutive frames as inputs to generate future frames. Compared with reconstruction-based methods [18], [19] that expect outputs to be consistent with inputs, these methods have a greater advantage in exploiting the coherence of neighboring frames. As a result, prediction-based methods have achieved superior performance generally and have received more focus in recent years.

However, existing prediction-based methods typically consider only local or global normality. This single normality is hard to balance models' representation for normal and abnormal instances. In addition, the single normality is also difficult to generalize to various scenes because of the diversity of normal and abnormal patterns in different scenes. Many of prediction-based methods [4], [17], [22], [23] over-focus on local normality. They tend to capture spatiotemporal representations from current input frame sequence utilizing delicately designed prediction models. According to the spatiotemporal representations, they can learn the evolution regularities of consecutive frames and consider the regularities as local normality to infer future frames. For example, Frame-Pred [22] uses a fine-tuned U-Net [24] to capture the spatial representations of four consecutive frames while considering

optical flow as temporal information to generate the fifth frame. In addition, adversarial training is added to Frame-Pred to generate more realistic predicted frames. Therefore, the methods over-focusing on local normality often have excellent prediction ability and can represent more diverse and complex normal patterns. However, the powerful prediction ability also allow them to predict some anomalies instances well and cause missed detections [15]. In some simper scenes, abnormal events may be easily predicted due to their simple evolution regularities, which will leads to more missed detections.

In contrast, some prediction-based methods [15], [25] over-focus on global normality. In training phase, they attempt to record the prototype features of all normal videos by external memories to memorize global prototypical patterns. In testing phase, they consider the prototypical patterns as the learned global normality and perform the prediction task utilizing the prototype features to constrict the prediction ability for anomalies. Although the methods can limit the generalization for anomalies by global normality, they almost ignore the importance of local spatiotemporal representations. It has been revealed by many excellent work [26], [27] that local spatiotemporal representations are crucial for models to understand videos. Therefore, the methods over-focusing global normality also restricts their representation for normal instances and causes false alarms. Seriously, the false alarms may be more frequent in complex or larger datasets due to the diversity and complexity of normal patterns.

To address above issues, we proposed a two-branch VAD model, Local-Global Normality Network (LGN-Net), to take into account both local and global normality of training videos. Specifically, one branch captures local spatiotemporal representations with a unified cell to learn the evolution regularities of appearance and motion in consecutive frames while the other branch memorizes prototype features with a memory module and updates them using all normal videos to learn the global prototypical patterns. To fuse the local and global normality, we combine the local spatiotemporal representations and the updated prototype features to generate future frames utilizing a unified decoder. Benefiting from the two-branch strategy, LGN-Net achieves a balance that allows LGN-Net to represent diverse and complex normal patterns while constricting its prediction for anomalies. In addition, the fused normality also enables LGN-Net more generalized to various scenes compared to exploiting single normality. Experiments demonstrate the effectiveness of the proposed methods.

Different from existing methods that take optical flow as motion information [22], [25], [28], we capture appearance and motion evolution from video frames with a unified cell in the spatiotemporal branch inspired by PredRNN [26] and PredRNN-V2 [27]. Therefore, the spatiotemporal branch allows our model to abandon optical flow, which reduces the computational cost and frees our model from relying on optical flow networks. In addition, many methods [3], [22], [23] utilize U-Net [24] or deep autoencoder to capture local representation from consecutive frames, but these backbone networks are not adept at processing temporal sequence data. To this end, we design the spatiotemporal branch based on the recurrent

neural network, which enables our model to be more adept at learning temporal variation. Unlike MemAE [19] and LMC-Net [29], we utilize a memory module with new update and query schemes in prototype branch inspired by MNAD [15] to avoid excessive restrictions on representing normal patterns.

The contributions of this paper are summarized as follows:

- We introduce a novel VAD method to consider local and global normality of training videos simultaneously, which solves the inherent problem that existing VAD methods have difficulty in balancing their representation capacity for normal and abnormal patterns.
- We propose a two-branch model named LGN-Net, where one branch learns the evolution regularities of appearance and motion and the other branch memorizes normal prototype features. The two-branch strategy enables our model with excellent representation for normal patterns while limiting the model to represent anomalies.
- The experiments on benchmark datasets indicate our method is more adaptable to different datasets compared with state-of-the-art methods. In addition, we provide the comprehensive experimental analysis including visualization analysis and ablation studies. The code of our model is also available online.

The rest of this paper is organized as follows: In Section II, we summarize the relevant work in video anomaly detection. In Section III, we introduce the details of LGN-Net and the loss functions. In Section IV, we first introduce the evaluation metrics and the datasets used in our experiments. In addition, we conduct extensive experiments including comparison experiments, visualization analysis and ablation studies to validate the effectiveness of our method in the section. In Section V, we conclude the whole paper.

## II. RELATED WORK

In unsupervised VAD methods, the training sets are generally devised to contain only normal videos. In training phase, unsupervised VAD methods tend to learn the normality from training sets by performing a proxy task. In testing phase, any instance that significantly deviates from the normality will be considered as an abnormal instance [30]. The methods can be classified as reconstruction-based methods or prediction-based methods according to the proxy task performed.

### A. Reconstruction-based Methods

In reconstruction-based methods, models are usually designed based on autoencoder [15], [18], [19]. They typically utilize original video frames as ground truth and aim to achieve a trained autoencoder that makes the reconstruction error minimized. Due to only learning how to reconstruct normal frames in training phase, they assume that the reconstruction errors of abnormal frames will be higher than that of normal frames in testing phase. In recent years, many reconstruction-based VAD methods have been proposed [15], [18], [19], [21], [31], [32]. Hasan *et al.* [18] proposed to learn normal regularity in video frames using an autoencoder based on deep convolution neural network. Luo *et al.* [21] proposed a temporally-coherent sparse coding to force neighboring frames reconstructed by

similar reconstruction coefficients. Ravanbakhsh *et al.* [31] introduced a VAD model based on Generative Adversarial Network (GAN) [33]. They use normal frames to reconstruct corresponding optical flow images and use optical flow images to reconstruct corresponding normal frames. Compared with traditional VAD methods, reconstruction-based methods have made significant progress. However, due to the powerful representation of convolution neural network, sometimes they can reconstruct the abnormal frames with low errors as well. To this end, Gong *et al.* [19] devised a memory module for autoencoder inspired by memory network [34], which constrains model's ability to reconstruct abnormal frames by memorizing the prototypical elements of normal instances. Reconstruction-based methods have shown some good performance for VAD tasks, however, they almost ignore the temporal representations.

### B. Prediction-based Methods

In prediction-based VAD methods [15], [17], [22], [23], [25], [35], [36], the models usually take a number of consecutive video frames as input to generate the next frame. Compared with reconstruction-based methods, prediction-based VAD methods are more adept at exploiting spatiotemporal information among frames. Therefore, they are usually superior to reconstruction-based methods and have received more attention in recent years. Liu *et al.* [22] proposed the prediction-based VAD method, which utilizes four consecutive frames as input and predicts a future frame. They utilized the fine-tuned U-Net [24] as a generative model to generate future frames and devise a discriminator to enhance the prediction ability of the model. In addition, they take optical flow as motion (temporal) information to help the model generate more realistic future frames. Lee *et al.* [17] proposed a VAD model named STAN, which consists of a ConvLSTM-based [37] generator and a spatiotemporal discriminator. Park *et al.* [15] devised a new memory module for VAD model to record normal prototype features, which can represent more diverse patterns than the memory module in MemAE [19]. They use normal prototype features to represent predicted frames, which limit the prediction ability for abnormal events. In recently, many two-stream models have been proposed [23], [25], [36], which often utilize two branches to learn spatial and temporal normal patterns separately. Chang *et al.* [36] devised a two-stream model consisting of spatial autoencoder and temporal autoencoder to dissociate the spatiotemporal representations. The model performs the reconstruction task using spatial autoencoder to learn appearance normal patterns while performing the prediction task using a temporal autoencoder based on U-Net to learn motion normal patterns. Cai *et al.* [25] attempted to explore spatiotemporal consistency and proposed a two-stream model named AMMC-Net. They designed two autoencoders with memory module, one with frames as input for learning appearance normal patterns and the other with the optical flow as input for learning motion normal patterns. Hao *et al.* [23] introduce a model named STCEN, composed of a 3D CNN-based encoder and a 2D CNN-based decoder, to extract motion and appearance fusion features. In this work,

a 3D CNN-based discriminator is devised to force predicted frames to be more realistic.

Although the above methods have made efforts in learning spatiotemporal representations and achieve better performance, they are almost incapable of taking into account both local and global normality of training videos. Many of them [17], [22], [23], [36] focus on learning local normality and enhancing prediction ability by exploiting appearance and motion information or devising a discriminator for generative model. The powerful prediction ability enable them to represent some abnormal instances well. Besides, many prediction-based methods [15], [25] tend to record global normal patterns while ignoring local spatiotemporal representation.

## III. THE PROPOSED METHOD

Anomalies in videos can be defined as unexpected behavior or the behavior deviating from normal patterns [38]. Based on this definition, we introduce an unsupervised VAD method aiming to learn both local and global normality from training sets consisting of only normal videos by performing a prediction task. The instances deviating from the normality will achieve high prediction error and thus are regarded as anomalies. Specifically, we propose a two-branch model, where one branch aims to learn the evolution regularities of appearance and motion from several consecutive frames and considers the regularities in this short term as local normality while the other branch updates the prototype features recorded in a memory pool using whole training videos and consider the prototypes as global normality.

### A. Overall Framework

As shown in Fig. 2, the proposed LGN-Net consists of spatiotemporal branch and prototype branch. We denote the video frame sequence as  $S = \{s_{t-n+1}, s_{t-n+2}, \dots, s_t\}$ , which contains  $n$  consecutive video frames. In the spatiotemporal branch, we first feed the sequence  $S$  to the encoder  $E_{loc}$  and denote frames  $\{s_{t-n+1}, s_{t-n+2}, \dots, s_t\}$  after encoding as  $\{x_{t-n+1}, x_{t-n+2}, \dots, x_t\}$ . Then,  $x$  is input to the spatiotemporal prediction network (STP-Net) in time step order, which is a convolutional recurrent neural network aiming to capture the spatial and temporal representations within a unified cell. We denote the final spatiotemporal memory and the final hidden state of STP-Net as  $M$  and  $H$  respectively, which contain the spatiotemporal representations from time step  $t-n+1$  to  $t$  in  $S$ . Therefore, we concatenate  $M$  and  $H$  as the local spatiotemporal feature  $F_{loc}$  finally. In the prototype branch, we first feed the frame sequence  $S$  to the encoder  $E_{glo}$  to generate latent space features  $F_{lat}$ . Then,  $F_{lat}$  is expanded to a number of query features, which are used to update the prototype features recorded in the memory pool. The query features is represented approximately by combining updated prototype features according to a matching probability. After training phase, the prototype features will be updated by all sequences  $S$  from whole normal videos to memorize the global prototypical pattern, therefore the global feature  $F_{glo}$  is obtained by aggregating the reconstructed query features to constrict the representation for anomalies. Finally, the local

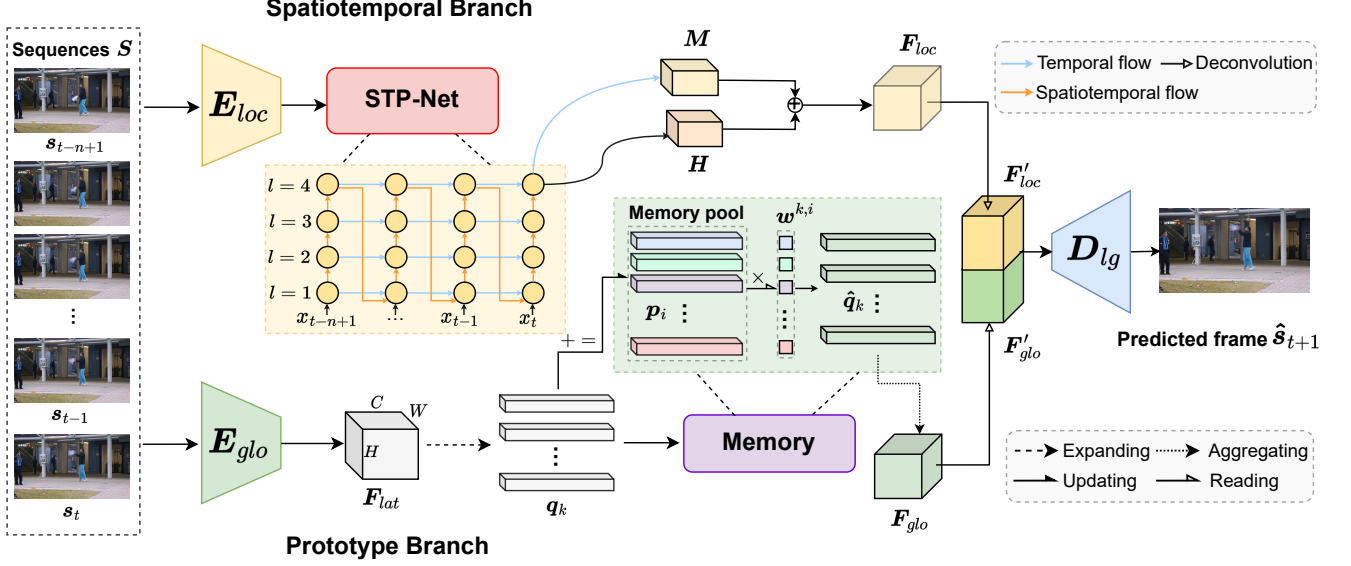


Fig. 2. The overall structure of LGN-Net. STP-Net consists of four ST-LSTM [26] units to model short-term evolution of appearance and motion without optical flow. The memory module aims to update the prototype features  $p_i$  recorded in the memory pool using all normal videos to learn global normality.  $w^{k,i}$  is a matching probability calculated based on the distance between  $q_k$  and  $p_i$ .

spatiotemporal features  $F_{loc}$  and the global features  $F_{glo}$  are concatenated after deconvolution and fed to the decoder  $D_{lg}$  to generate the next frame  $\hat{s}_{t+1}$ .

### B. Spatiotemporal Branch

We design the spatiotemporal branch to learn short-term evolution regularities of appearance and motion without optical flow inspired by PredRNN [27] and consider the regularities as local normality. As shown in Fig. 2, the spatiotemporal branch mainly consists of two components: the encoder  $E_{loc}$  and the spatiotemporal prediction network (STP-Net).  $E_{loc}$  is designed based on 2d convolutional neural networks, which aims to obtain the latent space features  $X = \{\mathbf{x}_{t-n+1}, \mathbf{x}_{t-n+2}, \dots, \mathbf{x}_t\}$  from sequence  $S$ . The STP-Net is a convolutional recurrent neural network that is employed to learn the local evolution regularities of appearance and motion.

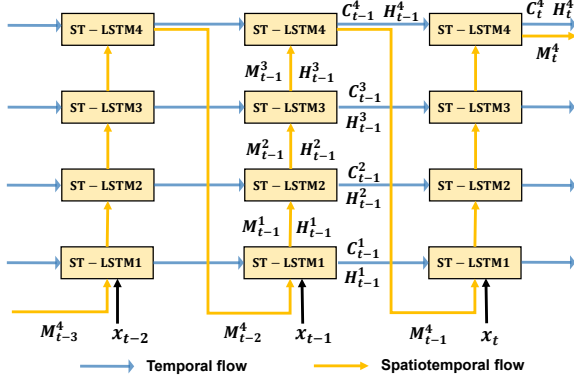


Fig. 3. Details of the STP-Net. The Spatiotemporal memory is updated in the zigzag direction, enabling the bottom unit (ST-LSTM<sub>1</sub>) to capture the spatial information output by the top unit (ST-LSTM<sub>4</sub>) at the previous time step.

Compared with deep autoencoder and U-Net [24] used in previous work [3], [22], [23], STP-Net is more adept at

learning temporal variations because of its recurrent structure. Furthermore, we utilize ST-LSTM [26] as the unit of STP-Net because it captures spatial and temporal representations within a unified cell and achieves superior performance over ConvLSTM [37] in appearance and motion prediction. Similar to ConvLSTM [37], the temporal cell  $C_t^l$  in STP-Net is updated horizontally from the previous time step to the current time step within all layers as shown in Fig. 3. In addition to  $C_t^l$ , ST-LSTM devised a spatiotemporal memory cell  $M_t^l$  to model both spatial and temporal features. For the bottom of STP-Net, spatiotemporal memory conveyed from the top layer at previous time step to the bottom layer at current time step, denoted as  $M_t^0 = M_{t-1}^4$ . For the other layers, spatiotemporal memory is transmitted from  $l-1$  layer to the current layer vertically at the same time step. Therefore, the zigzag direction update strategy enables STP-Net to overcome the layer-independent memory mechanism in ConvLSTM [37] and memorize the evolution regularities of appearance and motion in a unified memory cell. The key equations of STP-Net are shown as follows:

$$\begin{aligned}
 i_t &= \sigma(W_i^x * \mathbf{x}_t + W_i^h * \mathbf{H}_{t-1}^l) \\
 f_t &= \sigma(W_f^x * \mathbf{x}_t + W_f^h * \mathbf{H}_{t-1}^l) \\
 i'_t &= \sigma(W_{im}^x * \mathbf{x}_t + W_{im}^m * M_t^{l-1}) \\
 f'_t &= \sigma(W_{fm}^x * \mathbf{x}_t + W_{fm}^m * M_t^{l-1}) \\
 C_t^l &= f_t \odot C_{t-1}^l + i_t \odot \tanh(W_c^x * \mathbf{x}_t + W_c^h * \mathbf{H}_{t-1}^l) \\
 M_t^l &= f'_t \odot M_t^{l-1} + i'_t \odot \tanh(W_m^x * \mathbf{x}_t + W_m^m * M_t^{l-1}) \\
 o_t &= \sigma(W_o^x * \mathbf{x}_t + W_o^h * \mathbf{H}_{t-1}^l + W_o^c * C_t^l + W_o^m * M_t^l) \\
 \mathbf{H}_t^l &= o_t \odot \tanh(W_{1 \times 1} * [C_t^l, M_t^l]),
 \end{aligned} \tag{1}$$

where  $*$  and  $\odot$  denote the convolution operator and the

Hadamard product respectively.  $\sigma$  is the sigmoid activation function.  $i_t$  and  $f_t$  are the input gate and forget gate of temporal cell respectively, while  $i'_t$  and  $f'_t$  are the input gate and forget gate of spatiotemporal cell respectively.

As shown in Fig. 3, in order to learn the evolution regularities of appearance and motion in  $S$ , we feed every  $x$  individually into STP-Net in time step order. According to Eq. 1, we can learn that the final spatiotemporal memory  $M_t^4$  contains the spatiotemporal information from the past time step to the current time step and the final hidden state  $H_t^4$  consider both standard temporal memory and spatiotemporal memory. Therefore, we concatenate  $H_t^4$  and  $M_t^4$  together as the local spatiotemporal representations  $F_{loc}$  of the current input sequence. Note that we denote  $H_t^4$  and  $M_t^4$  as  $H$  and  $M$  respectively in Fig. 2. The local spatiotemporal representations made it unnecessary to use optical flow as motion information, which only tends to represent variations between adjacent frames [39] and results in higher computational cost. LGN-Net explore complete evolution regularities of appearance and motion from input frame sequence by the spatiotemporal branch.

### C. Prototype Branch

We design the prototype branch to memorize the prototype features with a memory module from whole training videos inspired by MNAD [15] and consider the prototypes as global normality. As shown in Fig. 2, the prototype branch is designed based on a memory-augmented deep autoencoder. The branch mainly consists of three components: the encoder  $E_{glo}$ , the memory module, and the decoder  $D_{lg}$ . The encoder  $E_{glo}$  is designed based on 2d convolutional neural networks, which takes the sequence  $S$  as input and outputs the latent space features  $F_{lat} \in \mathbb{R}^{H \times W \times C}$ . The memory module record prototype features in a memory pool and updates them utilizing  $F_{lat}$  from whole training videos to memorize global prototypical patterns. Therefore, we can consider the updated prototype features as learned global normality in testing phase. We represent  $F_{lat}$  approximately using the updated prototype features to limit the representation for anomalies and denote it as  $F_{glo}$ .  $F_{glo}$  and  $F_{loc}$  have the same dimension after deconvolution, denoted as  $F'_{glo}$  and  $F'_{loc}$  respectively. Finally, we concatenate  $F'_{glo}$  and the  $F'_{loc}$  to fuse local and global normality, and then feed them into the decoder  $D_{lg}$  to generate a future frame  $\hat{s}_{t+1}$ .

In the memory module, the latent space features  $F_{lat}$  are expanded into a number of query features, denoted as  $q_k \in \mathbb{R}^C (k = 1, 2, \dots, K)$ , where  $K = H \times W$ . The memory module records a number of prototype features with the same dimension as feature  $q_k$ , denoted as  $p_i \in \mathbb{R}^C (i = 1, 2, \dots, I)$ . The query scheme of memory module determines how to represent  $q$  using the recorded  $p$  approximately, while the update scheme describes how to update  $p$  using the current  $q$ .

In the query scheme, we compute the similarity between  $q$  and  $p$  using the cosine similarity and then apply a softmax

function vertically on it to obtain matching probability  $w^{k,i}$ :

$$w^{k,i} = \frac{\exp \left( (\mathbf{p}_i)^T \mathbf{q}_k \right)}{\sum_{i'=1}^I \exp \left( (\mathbf{p}_{i'})^T \mathbf{q}_k \right)}. \quad (2)$$

To represent  $q_k$  approximately, we obtain  $\hat{q}_k$  using a linear combination of all the prototype features  $p$  according to  $w^{k,i}$  as shown in Eq. 3. Then, all  $\hat{q}_k$  corresponding to  $q_k$  are aggregated and denoted as the global feature  $F_{glo}$  to represent  $F_{lat}$  approximately.

$$\hat{q}_k = \sum_{i'=1}^I w^{k,i'} \mathbf{p}_{i'}. \quad (3)$$

In the update scheme, all query features claiming to be nearest to the prototype feature according to the matching probabilities in Eq. 2 are selected to update it. We use  $U^i$  to denote the set of query features for updating  $p_i$ . A weighted average of the query features is used to update  $p_i$  to memorize the prototype features:

$$\hat{p}_i = \left\| \mathbf{p}_i + \sum_{k \in U^i} v_u^{k,i} \mathbf{q}_k \right\|_2. \quad (4)$$

Similar to Eq. 2, we apply the softmax function in the horizontal direction to obtain  $v^{k,i}$ :

$$v^{k,i} = \frac{\exp \left( (\mathbf{p}_i)^T \mathbf{q}_k \right)}{\sum_{k'=1}^K \exp \left( (\mathbf{p}_i)^T \mathbf{q}_{k'} \right)}. \quad (5)$$

Then,  $v^{k,i}$  is renormalized to consider the query features in  $U^i$ :

$$v_u^{k,i} = \frac{v^{k,i}}{\max_{k' \in U^i} v^{k',i}}. \quad (6)$$

Additionally, in testing phase, the prototype features may also be updated by some frames in testing videos, which allows our model to make more adequate use of testing videos. We use a weighted regular score to prevent the prototype features from updating by abnormal instances.  $R_t$  is used to denotes the regular score of  $s_t$ :

$$R_t = \sum_{i,j} W_{ij} (\hat{s}_t, s_t) \left\| \hat{s}_t^{i,j} - s_t^{i,j} \right\|_2, \quad (7)$$

where the weight function  $W_{ij}$  is represented as follows:

$$W_{ij} (\hat{s}_t, s_t) = \frac{1 - \exp \left( - \left\| \hat{s}_t^{i,j} - s_t^{i,j} \right\|_2 \right)}{\sum_{i,j} 1 - \exp \left( - \left\| \hat{s}_t^{i,j} - s_t^{i,j} \right\|_2 \right)}, \quad (8)$$

and  $i, j$  are the spatial indices of pixels. We set a threshold  $\gamma$  and consider the frames with regular score  $R_t$  higher than  $\gamma$  as abnormal frames, and do not use these frames to update the prototype features.

#### D. Training loss

To train our model, we introduce three loss functions: intensity loss, compactness loss, and separateness loss.

The intensity loss  $\mathcal{L}_{int}$  is calculated based on L2-norm to ensure the similarity of the pixels between a predicted frame  $\hat{s}$  and its corresponding ground truth  $s$ :

$$\mathcal{L}_{int}(\hat{s}, s) = \|\hat{s} - s\|_2. \quad (9)$$

The compactness loss  $\mathcal{L}_{com}$  aims to reduce the distance between the query feature  $q_k$  and its closest prototype feature  $p_c$ , which enables the prototype features have superior representation. The feature compactness loss is shown as follows:

$$\mathcal{L}_{com} = \sum_k^K \|q_k - p_c\|_2, \quad (10)$$

where  $c$  is the index of the prototype feature closest to  $q_k$ .

To ensure excellent representation capability after linear combination, the prototype features recorded in the memory pool should be separated from each other adequately. Therefore, we utilize the separateness loss  $\mathcal{L}_{sep}$  in this work, defined with a margin of  $\alpha$  as:

$$\mathcal{L}_{sep} = \sum_k^K [\|q_k - p_c\|_2 - \|q_k - p_s\|_2 + \alpha]_+, \quad (11)$$

where  $s$  is the index of prototype feature second closest to  $q_k$ , and  $\alpha$  is a constant.

The final training loss  $\mathcal{L}_{lgn}$  of our proposed model considers all the above loss functions, which can be represented as follow:

$$\mathcal{L}_{lgn} = \mathcal{L}_{int} + \lambda_c \mathcal{L}_{com} + \lambda_s \mathcal{L}_{sep}, \quad (12)$$

where  $\lambda_c$  and  $\lambda_s$  are used to balance each loss in the final objective function.

#### E. Normality Score

In testing phase, we quantify the extent of normality using normality score for each frame. Normality scores are usually calculated based on the difference between predicted frames and the corresponding ground truth [17], [22]. In this work, we calculate normality score utilizing peak signal to noise ratio (PSNR) and the difference between query features and prototype features.

PSNR has proven to be an effective measure in past work [40]. The PSNR between a predicted frame  $\hat{s}_t$  and its corresponding ground truth  $s_t$  can be shown as follows:

$$P(\hat{s}_t, s_t) = 10 \log_{10} \frac{\max(\hat{s}_t)}{\|\hat{s}_t - s_t\|_2^2 / N}, \quad (13)$$

where  $N$  is the number of pixels in  $s_t$ .

We compute the L2 distance between each query feature and its closest prototype feature as the difference, which reflects the deviation extent of the input instance from the global normality:

$$D(\mathbf{q}, \mathbf{p}) = \frac{1}{K} \sum_k^K \|q_k - p_c\|_2, \quad (14)$$

where  $p_c$  is the the closest prototype feature to  $q_k$ .

Then, we normalize PSNR and distance  $D$  to  $[0, 1]$ :

$$S_t = \lambda (1 - g(P(\hat{s}_t, s_t))) + (1 - \lambda)g(D(\mathbf{q}, \mathbf{p})), \quad (15)$$

where  $\lambda$  is used to balance PSNR and distance  $D$ .  $g(\cdot)$  is a normalization function,which can be shown as follows:

$$g(P(\hat{s}_t, s_t)) = 1 - \frac{P(s_t, \hat{s}_t) - \min_t P(s_t, \hat{s}_t)}{\max_t P(s_t, \hat{s}_t) - \min_t P(s_t, \hat{s}_t)}. \quad (16)$$

Finally, we obtain the normality score  $N_t$ , and a higher  $N_t$  means a lower prediction error:

$$N_t = 1 - S_t. \quad (17)$$

## IV. EXPERIMENTS

In order to validate the effectiveness of our method, we provide extensive experimental results and analysis in this section.

#### A. Evaluate Metrics and Benchmark Datasets

**Evaluation Metrics.** To quantitatively evaluate our method, following the previous work [15], [19], [22], we calculate the receiver operating characteristic (ROC) curve and utilize the average area under the curve (AUC) as the evaluation metrics. In this work, we use frame-level AUC to evaluate performance of VAD methods, and the higher AUC indicates the superior performance.

**Benchmark Datasets.** We performed experiments on three benchmark datasets, including UCSD Ped2 [20], CUHK Avenue [43] and ShanghaiTech [21], which have been used in many excellent VAD work [7], [15], [19], [22].

- **UCSD Ped2** [20] contains 16 training and 12 testing videos. The dataset is captured on pedestrian walkways in university of California San Diego. In the dataset, the normal and abnormal patterns are relatively simple. The dataset defines walking pedestrians as normal and considers events such as bicycling and skateboarding as abnormal.
- **CUHK Avenue** [43] dataset includes 37 videos consisting of about 30,000 frames in total, where 21 testing videos including abnormal events. In the dataset, normal patterns are also simple similar to UCSD ped2. However, abnormal patterns in this dataset are more difficult than UCSD ped2, which contains a variety of abnormal events such as fast running, throwing and loitering.
- **ShanghaiTech** [21] dataset consists of 330 training videos and 107 testing videos. This dataset is much more complex and larger compared with UCSD ped2 and CUHK Avenue. This dataset contains a large amount of video data and was captured in 13 different scenes, which lead to the normal patterns in it being diverse and complex. In addition, the dataset contains a variety of complex abnormal events, such as chasing, fighting and robbing.

TABLE I

RESULTS OF QUANTITATIVE FRAME-LEVEL AUC (%) COMPARISON. BOLD NUMBERS INDICATE THE BEST PERFORMANCE, WHILE UNDERLINE ONES INDICATE THE SECOND BEST.

Types	Methods	UCSD Ped2	CUHK Avenue	ShanghaiTech
Traditional	MPPCA(Kim <i>et al.</i> , 2009) [41]	69.3	N/A	N/A
	MPCC+SFA(Mahadevan <i>et al.</i> , 2010) [20]	64.3	N/A	N/A
	MDT(Mahadevan <i>et al.</i> , 2010) [20]	82.9	N/A	N/A
Reconstruction	Conv-AE(Hasan <i>et al.</i> , 2016) [18]	85.0	80.0	60.9
	TSC(Luo <i>et al.</i> , 2017) [21]	91.0	80.6	67.9
	StackRNN(Luo <i>et al.</i> , 2017) [21]	92.2	81.7	68.0
	AbnormalGAN(Ravanbakhsh, <i>et al.</i> , 2017) [31]	93.5	N/A	N/A
	ConvLSTM-AE(Luo <i>et al.</i> , 2017) [32]	88.1	77.0	N/A
	MemAE(Gong <i>et al.</i> , 2019) [19]	94.1	83.3	71.2
Prediction	MNAD-Recon(Park <i>et al.</i> , 2020) [15]	90.2	82.8	69.8
	Frame-Pred(Liu <i>et al.</i> , 2018) [22]	95.4	84.9	72.8
	STAN(Lee <i>et al.</i> , 2018) [17]	96.5	87.2	N/A
	AMC(Nguyen <i>et al.</i> , 2019) [35]	96.2	86.9	N/A
	MESDnet(Zhou <i>et al.</i> , 2019) [42]	96.0	86.0	N/A
	Multispace(Zhang <i>et al.</i> , 2020) [4]	95.4	86.8	73.6
	MNAD(Park <i>et al.</i> , 2020) [15]	97.0	88.5	70.5
	AMMC-Net(Cai <i>et al.</i> , 2021) [25]	96.6	86.6	73.7
	STD(Chang <i>et al.</i> , 2022) [36]	96.7	87.1	73.7
	STCEN(Hao <i>et al.</i> , 2022) [23]	96.9	86.6	<b>73.8</b>
	LGN-Net(Ours)	<b>97.1</b>	<b>89.3</b>	73.0

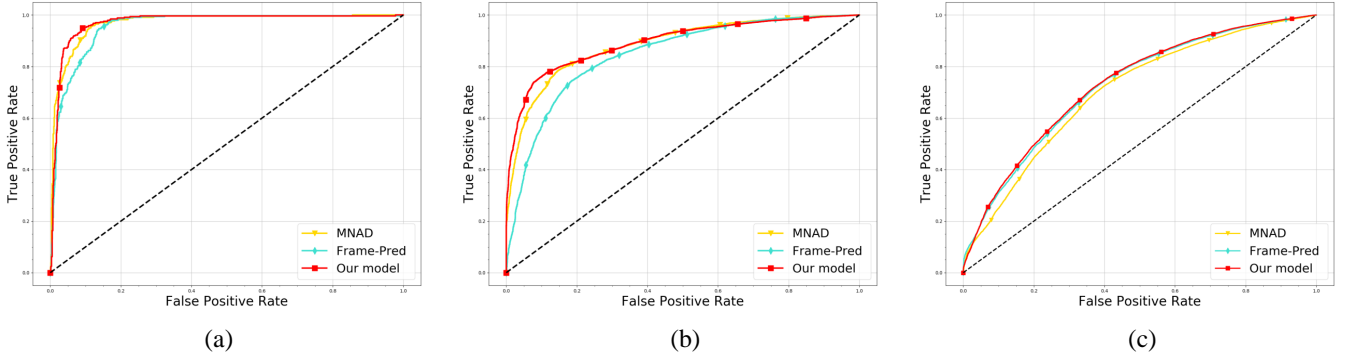


Fig. 4. Frame-level ROC curves of our model, Frame-Pred [22] and MNAD [15] on UCSD Ped2 (a), CUHK Avenue (b), and ShanghaiTech (c) datasets.

### B. Implementation Details

In the experiments, all frames are resized to  $256 \times 256$  and the intensity of pixels is normalized to  $[-1, 1]$ . We use Adam [44] to optimize our model with a batch size of 8. The learning rate of LGN-Net is set to  $2 \times 10^{-4}$  and  $\alpha$  is set to 1.  $n$  is set to 4, which means we use four consecutive frames to predict the fifth frame in the prediction task. The dimension of  $\mathbf{x}_t$  in the spatiotemporal branch is set to  $64 \times 64 \times 128$ .  $H$ ,  $W$  and  $C$  are set to 32, 32 and 512, respectively, which means the dimension of latent space features  $\mathbf{F}_{lat}$  in the prototype branch is  $32 \times 32 \times 512$ .

When processing simple datasets, the representation capability of LGN-Net needs to be strictly limited to prevent predicting simple abnormal instances well. Therefore, for UCSD ped2 [20] and CUHK Avenue [43],  $I$  is set to 10, which means the memory module only record ten normal prototype features. Correspondingly, for ShanghaiTech [21],  $I$  is set to 200 so as to represent the complex and diverse normal patterns. For UCSD ped2, CUHK Avenue and ShanghaiTech,  $\lambda_c$  is set

to 10, 10 and 1,  $\lambda_s$  is set to 5, 2 and 1,  $\lambda$  is set to 0.6, 0.5 and 0.8, and  $\gamma$  is set to 0.009, 0.006 and 0.0135, respectively.

### C. Comparison with Existing Methods

In this section, we compared our method with some existing state-of-the-art methods on three benchmark VAD datasets mentioned above. The methods involved in the comparison experiment can be classified as traditional methods [20], [41], reconstruction-based (Reconstruction) methods [15], [18], [19], [21], [31], [32] and prediction-based methods (Prediction) [4], [15], [17], [22], [23], [25], [35], [36], [42]. The proposed method belongs to prediction-based methods. We report the frame-level AUC (%) of all the methods and the comparison results are presented in Table I.

The traditional methods in Table I extracts features using hand craft and tend to employ a one-class classifier to perform classification tasks. This results in these methods are not robust in complex scenes and large datasets. Therefore, compared

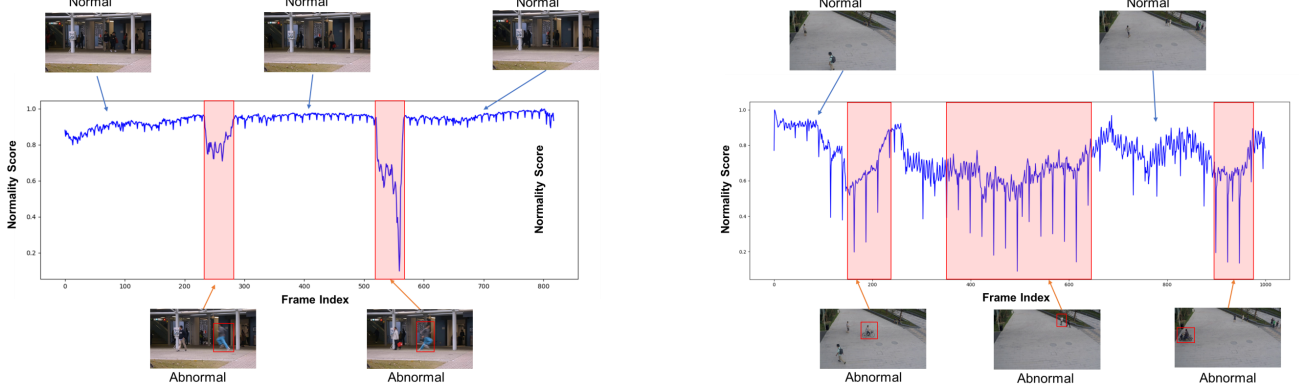


Fig. 5. Normality scores on two testing video clips from CUHK Avenue [43] (left) and ShanghaiTech [21] (right) datasets. The period of the abnormal events are marked by red regions. In CUHK Avenue (left), both of the two abnormal events are fast running. In ShanghaiTech (right), the three abnormal events are bicycle riding, skateboarding, and motorcycle riding in temporal order.

with these methods, reconstruction-based and predication-based methods achieve superior performance significantly.

Compared with reconstruction-based methods, prediction-based methods are usually more adept at exploiting spatiotemporal information among frames. Therefore, as shown in Table I, the prediction-based methods are superior to reconstruction-based methods generally. Compared with reconstruction-based methods, LGN-Net achieved significantly superior performance as well.

The prediction-based methods have made lots of efforts in learning normality from training videos. However, all these methods have difficulty in taking into account both local and global normality of videos, while favoring one of them. MNAD [15] utilizes a memory module to memorize global prototype features and almost ignore local spatiotemporal representation. This causes MNAD [15] has difficulty representing diverse and complex normal patterns in ShanghaiTech dataset and achieves 70.5% AUC only. Compared with MNAD [15], LGN-Net capture local spatiotemporal representations using the spatiotemporal branch, which enables it having a significant advantage in representing diverse and complex patterns. Therefore, it achieves remarkably superior performance (2.5% AUC gain) compared with MNAD [15] on ShanghaiTech [21]. Compared to our model, although AMMC-Net [25] achieves a 0.7% AUC gain on ShanghaiTech, it suffers a 2.7% AUC decrease on CUHK Avenue. In addition, AMMC-Net needs to calculate the corresponding optical flow for all frames as temporal information.

Frame-Pred [22], Multispace [4], STAN [17] and STCEN [23] over-focus on local normality. They tend to improve models' prediction ability by exploiting local spatial and temporal information and utilize adversarial training [33] to enhance the learned local normality. The learned local normality enables them to represent more complex normal patterns, thus Frame-Pred [22], Multispace [4] and STCEN [23] achieve remarkable performance on ShanghaiTech [21]. However, the strong representation ability allow them to represent some simple abnormal patterns well potentially [19], which leads to their relatively poor performance on UCSD ped2 [20] and CUHK Avenue [43]. Compared to these methods, LGN-Net

can limit the representation capability for the simple abnormal instances in UCSD ped2 and CUHK Avenue utilizing recorded normal prototype features and therefore achieves remarkably superior performance on these datasets.

In Fig. 4, we compared our model with other models in terms of the frame-level ROC curves. The comparison clearly demonstrates our model achieve superior performance compared to Frame-Pred [22] on UCSD ped2 [20] and CUHK Avenue [43]. In addition, the comparison also indicates that our model achieves significantly superior performance compared to MNAD [15] on ShanghaiTech [21]. Since the code of some recent excellent methods are not available now, we choose these two methods for the comparison. Frame-Pred and MNAD are well known and have excellent performance in VAD task, and they are over-focusing on local and global normality respectively.

In conclusion, compared with the methods in Table I, LGN-Net is more adaptable to various scenes with different complexity. It achieves the best performance on UCSD ped2 [20] and CUHK Avenue [43] while also achieving competitive performance in the more complex ShanghaiTech [21].

#### D. Visualization Analysis

In order to further demonstrate the effectiveness of our method on VAD task, we provide the visualization result of LGN-Net. In addition, the visualization result could help our model to infer the time and position of abnormal events.

In Fig. 5, we visualize normality scores output by LGN-Net on two testing video clips from CUHK Avenue [43] and ShanghaiTech [21]. As mentioned in Section III-E, the higher normality score in Fig. 5 means the lower prediction error and the lower score means the higher error at that time. As shown in Fig. 5, during normal events the normality score remains stable and relatively higher. However, during abnormal events, the normality score drops drastically on these two videos. Thus, this visualization result further demonstrates the effectiveness of LGN-Net for abnormal event detection and also helps LGN-Net to infer the periods in which abnormal events are occurring.

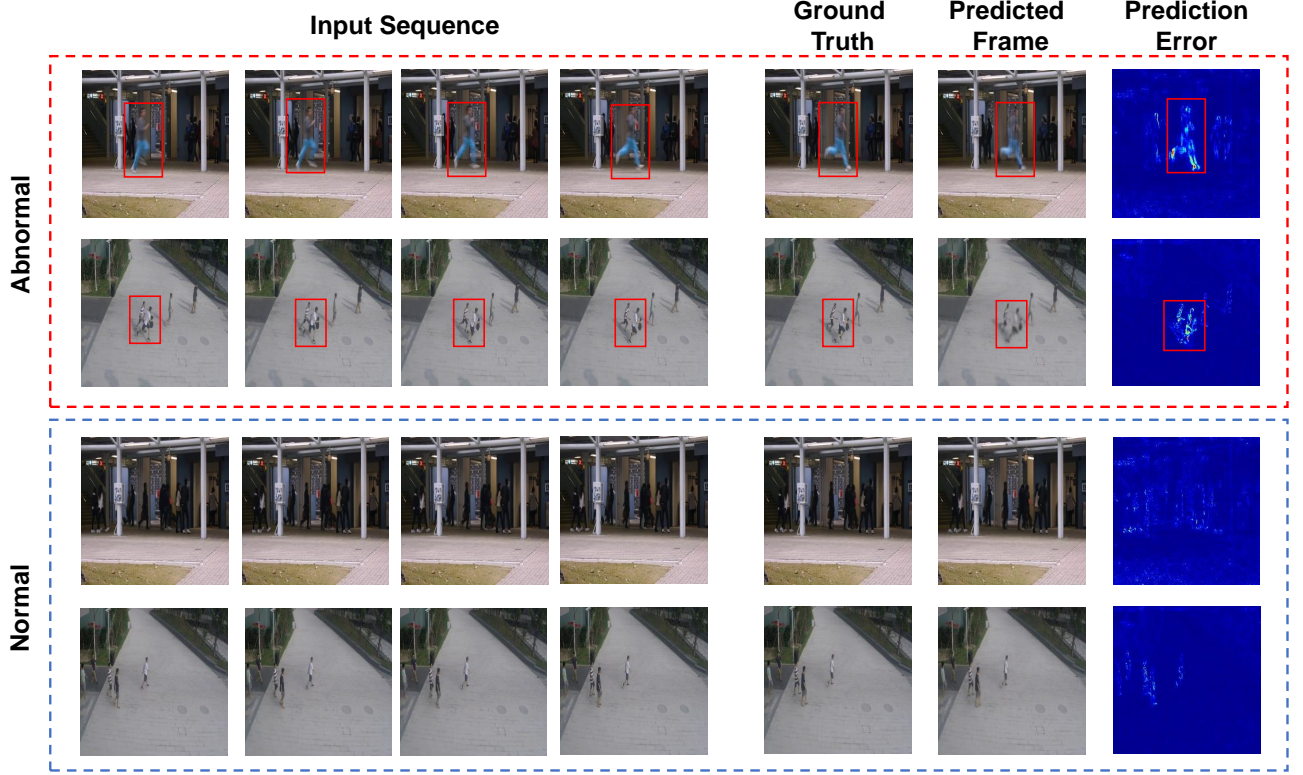


Fig. 6. Visualization of predicted frames and prediction errors. The first and third rows are the visualization results on CUHK Avenue [43], while the second and fourth rows are on ShanghaiTech [21]. The abnormal events in the first and second rows are fast running and fighting respectively. The red bounding boxes are used to mark the positions of abnormal events. The brighter color in the rightmost column denotes the larger prediction error.

TABLE II  
QUANTITATIVE COMPARISON FOR VARIANTS OF OUR MODEL. WE MEASURE THE FRAME-LEVEL AUC (%) ON THE CUHK AVENUE [43] AND SHANGHAITECH [21]. BOLD NUMBER INDICATES THE BEST PERFORMANCE.

Model	Spatiotemporal Branch	Prototype Branch	ST-LSTM	CUHK Avenue (AUC)	ShanghaiTech (AUC)
Loc-Net	✓	✗	✗	84.7	71.4
Glo-Net	✗	✓	✗	88.5	70.3
LGN-ST	✓	✓	✗	88.8	72.1
LGN-Net(Ours)	✓	✓	✓	<b>89.3</b>	<b>73.0</b>

In Fig. 6, we visualize prediction errors output by LGN-Net on four instances from CUHK Avenue [43] and ShanghaiTech [21]. The prediction error is the difference between a predicted frame and its corresponding ground truth. As shown in Fig. 6, prediction errors are very obvious in abnormal events, corresponding to the upper part of the figure. However, the predicted frames are remarkably close to the ground truth in the normal events, and thus the prediction errors are quite slight, corresponding to the lower part of the figure. We use red bounding boxes to mark the most obvious parts of the prediction errors in the rightmost column, which are exactly the positions of abnormal objects. Therefore, this visualization result further demonstrates the effectiveness of LGN-Net for abnormal objects detection and helps LGN-Net to infer the spatial positions of abnormal events.

#### E. Ablation Studies

To further demonstrate the effectiveness of our method, we conduct ablation analysis in this section. We report the frame-

level AUCs of LGN-Net and its variants on CUHK Avenue [43] and ShanghaiTech [21] in Table II. Loc-Net and Glo-Net are baseline models. Loc-Net includes only spatiotemporal branch based on ConvLSTM [37], which results in it over-focusing on local normality. Glo-Net includes only prototype branch similar to MNAD [15], which results in it over-focusing on global normality. Similar to MNAD [15], we concatenate latent space features  $F_{lat}$  and the global features  $F_{glo}$  and feed them to the decoder  $D_{lg}$  in Glo-Net. LGN-ST contains spatiotemporal branch and prototype branch, but its STP-Net consist of ConvLSTM [37] rather than ST-LSTM [26]. In LGN-ST, we concatenate  $H_t^4$  and  $C_t^4$  as the final local spatiotemporal representations. LGN-Net is our final proposed model, which contains the two branches and utilizes ST-LSTM [26] as units of STP-Net.

Compared with Loc-Net, Glo-Net achieves a 3.8% AUC gain on CUHK Avenue [43] while getting a 1.1% AUC decrease on ShanghaiTech [21]. This further validates the methods over-focusing on global normality impose a limitation

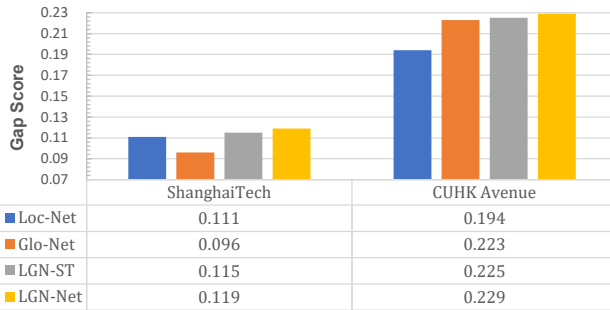


Fig. 7. Gap score of LGN-Net and its variants on ShanghaiTech and CUHK Avenue. Gap score is the average normality score of normal frames minus that of the abnormal frames. The larger gap score indicates the better separability for normal and abnormal frames.

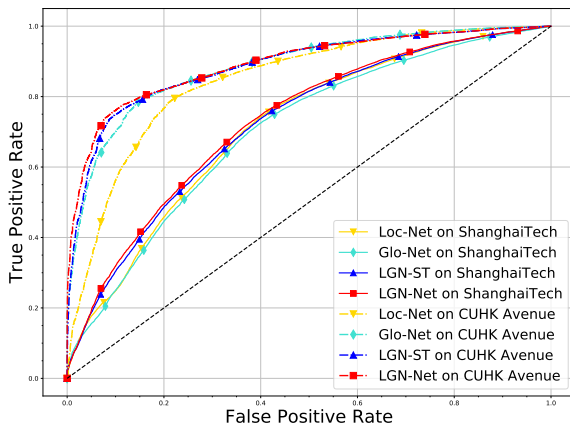


Fig. 8. Frame-level ROC curves of LGN-Net and its variants on ShanghaiTech [21] dataset.

on the representation for complex patterns. LGN-ST validates the effectiveness of local normality for diverse and complex patterns, it achieves a 1.8% AUC gain on ShanghaiTech compared to Glo-Net. In addition, LGN-ST achieves a 4.1% AUC gain on CUHK Avenue [43] compared to Loc-Net. This also indicates the effectiveness of global normality for the simpler dataset. LGN-Net achieves 0.5% and 0.9% AUC gains on CUHK Avenue and ShanghaiTech respectively compared to LGN-ST, which further shows the importance of local spatiotemporal representations for VAD task.

To further validate the effectiveness of local and global normality, we compared gap score and frame-level ROC curves of LGN-Net with its variants on CUHK Avenue and ShanghaiTech datasets. As shown in Fig. 7, LGN-Net achieves 0.004 and 0.023 gains in terms of the gap score compared to LGN-ST and Glo-Net respectively, which indicates that the local normality enables LGN-Net to have superior performance in separating normal and abnormal frames of ShanghaiTech [21] dataset. Furthermore, compared to Loc-Net, LGN-Net achieves a 0.035 gain in terms of the gap score, indicating that the global normality helps LGN-Net separate normal and abnormal frames of CUHK Avenue. In addition, Fig. 8 clearly indicates the effectiveness of devised components for the performance of LGN-Net on CUHK Avenue and ShanghaiTech datasets.

#### F. Hyperparameter Analysis

We proposed a threshold  $\gamma$  to select some normal frames from testing sets for updating the memory module in Section III-C, and set a parameter  $\lambda$  to balance PSNR and distance  $D$  in Eq. 15. In this section, as shown in Fig. 9 and Fig. 10, we report the AUC performance of LGN-Net with different  $\gamma$  and  $\lambda$  respectively on CUHK Avenue [43] and ShanghaiTech [21]. When we set  $\gamma$  to 0, which means the model does not use frames in testing videos to update the memory module. This lead to the model achieving 0.36% and 1.46% AUC decreases on CUHK Avenue and ShanghaiTech respectively compared with the best performances. When we set  $\lambda$  to 1, which means we only utilize PSNR to calculate the normality score. In this situation, the AUCs decreased by 4.34% and 1.92% on CUHK Avenue and ShanghaiTech respectively compared with the best performances. Therefore, these comparisons show the influence of parameters  $\gamma$  and  $\lambda$  on the performance of our model and also validate the effectiveness of these two strategies.

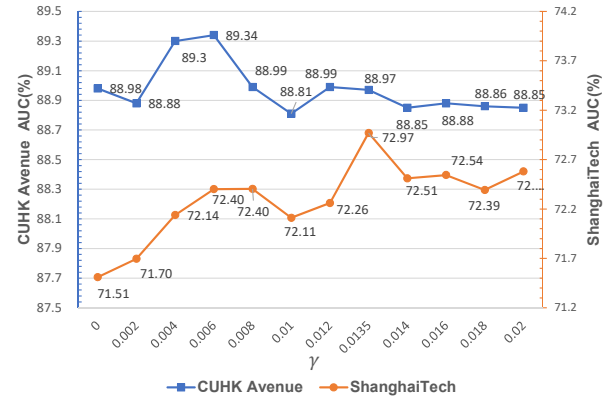


Fig. 9. Frame-level AUC (%) under different  $\gamma$  on CUHK Avenue [43] and ShanghaiTech [21] datasets. The blue curve indicates AUCs on CUHK Avenue and the orange curve indicates AUCs on ShanghaiTech.

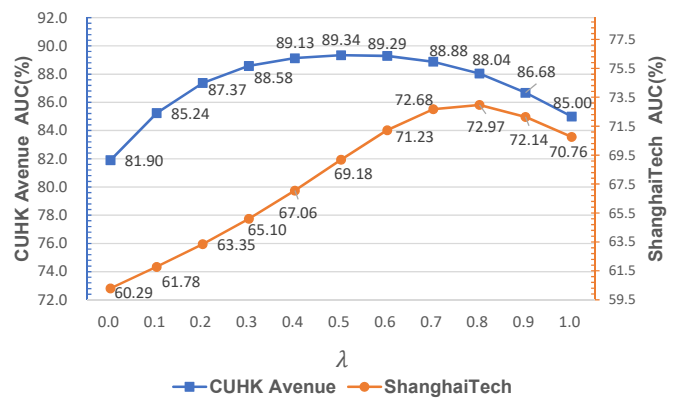


Fig. 10. Frame-level AUC (%) under different  $\lambda$  on CUHK Avenue [43] and ShanghaiTech [21] datasets. The blue curve indicates AUCs on CUHK Avenue and the orange curve indicates AUCs on ShanghaiTech.

### G. Running Time

When we evaluate our model on an Nvidia GTX TITAN Xp, the average running time is about 19 fps. On the same device, AnoPCN [12] achieves 10 fps, Frame-Pred [22] achieves 25 fps, STCEN [4] achieves 18 fps. This demonstrates that our model is also competitive with state-of-the-art methods in terms of running time.

### V. CONCLUSION

In this paper, we focus on the issue that most existing VAD methods over-focus only on local or global normality, making them difficult to balance the representation for normal and abnormal patterns and generalize to different scenes. To address this issue, we introduce a novel unsupervised VAD method to take into account both local and global normality. We propose a two-branch model named LGN-Net. One branch of the model learns spatiotemporal evolution regularities in consecutive frames as local normality and the other branch memorizes prototypical patterns of all normal videos as global normality. The local normality enable our model to understand more diverse and complex normal patterns while the global normality can limit the model's representation for abnormal instances. We enable the representation for normal and abnormal patterns to be more balanced by fusing the local and global normality, which helps VAD model more adaptable to various scenes with different complexity. Experiments demonstrate our method is competitive compared with state-of-the-art methods. In addition, related analysis further demonstrates the effectiveness of our method and devised components. In future work, we will try to explore a better way to consider local normality and global normality in VAD task.

### REFERENCES

- [1] L. Song, X. Hu, G. Zhang, P. Spachos, K. N. Plataniotis, and H. Wu, “Networking systems of ai: On the convergence of computing and communications,” *IEEE Internet Things J.*, vol. 9, no. 20, pp. 20352–20381, 2022.
- [2] X. Mo, V. Monga, R. Bala, and Z. Fan, “Adaptive sparse representations for video anomaly detection,” *IEEE Trans. Circuits Syst. Video Technol.*, vol. 24, no. 4, pp. 631–645, 2014.
- [3] J. Guo, P. Zheng, and J. Huang, “Efficient privacy-preserving anomaly detection and localization in bitstream video,” *IEEE Trans. Circuits Syst. Video Technol.*, vol. 30, no. 9, pp. 3268–3281, 2020.
- [4] Y. Zhang, X. Nie, R. He, M. Chen, and Y. Yin, “Normality learning in multispace for video anomaly detection,” *IEEE Trans. Circuits Syst. Video Technol.*, vol. 31, no. 9, pp. 3694–3706, 2021.
- [5] M.-I. Georgescu, A. Bărbălău, R. T. Ionescu, F. Shahbaz Khan, M. Popescu, and M. Shah, “Anomaly detection in video via self-supervised and multi-task learning,” in *Proc. IEEE/CVF Conf. Comput. Vis. Pattern Recognit.*, 2021, pp. 12737–12747.
- [6] M. I. Georgescu, R. T. Ionescu, F. S. Khan, M. Popescu, and M. Shah, “A background-agnostic framework with adversarial training for abnormal event detection in video,” *IEEE Trans. Pattern Anal. Mach. Intell.*, vol. 44, no. 9, pp. 4505–4523, 2022.
- [7] W. Luo, W. Liu, D. Lian, J. Tang, L. Duan, X. Peng, and S. Gao, “Video anomaly detection with sparse coding inspired deep neural networks,” *IEEE Trans. Pattern Anal. Mach. Intell.*, vol. 43, no. 3, pp. 1070–1084, 2021.
- [8] Y. Liu, J. Liu, M. Zhao, S. Li, and L. Song, “Collaborative normality learning framework for weakly supervised video anomaly detection,” *IEEE Trans. Circuits and Syst. II, Exp. Briefs*, vol. 69, no. 5, pp. 2508–2512, 2022.
- [9] Y. Liu, J. Liu, X. Zhu, D. Wei, X. Huang, and L. Song, “Learning task-specific representation for video anomaly detection with spatial-temporal attention,” in *Proc. IEEE Int. Conf. Acoust. Speech Signal Process.*, 2022, pp. 2190–2194.
- [10] Y. Chang, Z. Tu, W. Xie, and J. Yuan, “Clustering driven deep autoencoder for video anomaly detection,” in *Proc. Eur. Conf. Comput. Vis. Springer*, 2020, pp. 329–345.
- [11] Y. Liu, J. Liu, J. Lin, M. Zhao, and L. Song, “Appearance-motion united auto-encoder framework for video anomaly detection,” *IEEE Trans. Circuits and Syst. II, Exp. Briefs*, vol. 69, no. 5, pp. 2498–2502, 2022.
- [12] M. Ye, X. Peng, W. Gan, W. Wu, and Y. Qiao, “Anopcn: Video anomaly detection via deep predictive coding network,” in *Proc. 27th ACM Int. Conf. Multimedia*, 2019, p. 1805–1813.
- [13] D. Chen, L. Yue, X. Chang, M. Xu, and T. Jia, “Nm-gan: Noise-modulated generative adversarial network for video anomaly detection,” *Pattern Recognit.*, vol. 116, p. 107969, 2021.
- [14] Z. Fang, J. T. Zhou, Y. Xiao, Y. Li, and F. Yang, “Multi-encoder towards effective anomaly detection in videos,” *IEEE Trans. Multimedia*, vol. 23, pp. 4106–4116, 2021.
- [15] H. Park, J. Noh, and B. Ham, “Learning memory-guided normality for anomaly detection,” in *Proc. IEEE/CVF Conf. Comput. Vis. Pattern Recognit.*, 2020, pp. 14372–14381.
- [16] Y. Lai, R. Liu, and Y. Han, “Video anomaly detection via predictive autoencoder with gradient-based attention,” in *Proc. IEEE Int. Conf. Multimedia Expo*, 2020, pp. 1–6.
- [17] S. Lee, H. G. Kim, and Y. M. Ro, “Stan: Spatio-temporal adversarial networks for abnormal event detection,” in *Proc. IEEE Int. Conf. Acoust. Speech Signal Process.*, 2018, pp. 1323–1327.
- [18] M. Hasan, J. Choi, J. Neumann, A. K. Roy-Chowdhury, and L. S. Davis, “Learning temporal regularity in video sequences,” in *Proc. IEEE/CVF Conf. Comput. Vis. Pattern Recognit.*, 2016, pp. 733–742.
- [19] D. Gong, L. Liu, V. Le, B. Saha, M. R. Mansour, S. Venkatesh, and A. v. d. Hengel, “Memorizing normality to detect anomaly: Memory-augmented deep autoencoder for unsupervised anomaly detection,” in *Proc. IEEE/CVF Int. Conf. Comput. Vis.*, 2019, pp. 1705–1714.
- [20] V. Mahadevan, W. Li, V. Bhalodia, and N. Vasconcelos, “Anomaly detection in crowded scenes,” in *Proc. IEEE Conf. Comput. Vis. Pattern Recognit.*, 2010, pp. 1975–1981.
- [21] W. Luo, W. Liu, and S. Gao, “A revisit of sparse coding based anomaly detection in stacked rnn framework,” in *Proc. IEEE Int. Conf. Comput. Vis.*, 2017, pp. 341–349.
- [22] W. Liu, W. Luo, D. Lian, and S. Gao, “Future frame prediction for anomaly detection—a new baseline,” in *Proc. IEEE/CVF Conf. Comput. Vis. Pattern Recognit.*, 2018, pp. 6536–6545.
- [23] Y. Hao, J. Li, N. Wang, X. Wang, and X. Gao, “Spatiotemporal consistency-enhanced network for video anomaly detection,” *Pattern Recognit.*, vol. 121, p. 108232, 2022.
- [24] O. Ronneberger, P. Fischer, and T. Brox, “U-net: Convolutional networks for biomedical image segmentation,” in *Proc. Int. Conf. Med. Image Comput. Comput.-Assisted Intervention*. Springer, 2015, pp. 234–241.
- [25] R. Cai, H. Zhang, W. Liu, S. Gao, and Z. Hao, “Appearance-motion memory consistency network for video anomaly detection,” in *Proc. AAAI Conf. Artif. Intell.*, vol. 35, no. 2, 2021, pp. 938–946.
- [26] Y. Wang, M. Long, J. Wang, Z. Gao, and P. S. Yu, “Predrnn: Recurrent neural networks for predictive learning using spatiotemporal lstms,” in *Proc. 31th Int. Conf. Neural Inf. Process. Syst.*, 2017, pp. 879–888.
- [27] Y. Wang, H. Wu, J. Zhang, Z. Gao, J. Wang, P. Yu, and M. Long, “Predrnn: A recurrent neural network for spatiotemporal predictive learning,” *IEEE Trans. Pattern Anal. Mach. Intell.*, pp. 1–1, 2022.
- [28] Z. Liu, Y. Nie, C. Long, Q. Zhang, and G. Li, “A hybrid video anomaly detection framework via memory-augmented flow reconstruction and flow-guided frame prediction,” in *Proc. IEEE/CVF Int. Conf. Comput. Vis.*, 2021, pp. 13568–13577.
- [29] S. Lee, H. G. Kim, D. H. Choi, H. Kim, and Y. M. Ro, “Video prediction recalling long-term motion context via memory alignment learning,” in *Proc. IEEE/CVF Conf. Comput. Vis. Pattern Recognit.*, 2021, pp. 3054–3063.
- [30] Y. Lai, R. Liu, and Y. Han, “Video anomaly detection via predictive autoencoder with gradient-based attention,” in *Proc. IEEE Int. Conf. Multimedia Expo*, 2020, pp. 1–6.
- [31] M. Ravanbakhsh, M. Nabi, E. Sangineto, L. Marcenaro, C. Regazzoni, and N. Sebe, “Abnormal event detection in videos using generative adversarial nets,” in *Proc. IEEE Int. Conf. Image Process.*, 2017, pp. 1577–1581.
- [32] W. Luo, W. Liu, and S. Gao, “Remembering history with convolutional lstm for anomaly detection,” in *Proc. IEEE Int. Conf. Multimedia Expo*, 2017, pp. 439–444.

- [33] I. J. Goodfellow, J. Pouget-Abadie, M. Mirza, B. Xu, D. Warde-Farley, S. Ozair, A. C. Courville, and Y. Bengio, "Generative adversarial nets," in *Proc. 27th Int. Conf. Neural Inf. Process. Syst.*, 2014, pp. 2672—2680.
- [34] J. Weston, S. Chopra, and A. Bordes, "Memory networks," in *Proc. Int. Conf. Learn. Representations*, 2015.
- [35] T.-N. Nguyen and J. Meunier, "Anomaly detection in video sequence with appearance-motion correspondence," in *Proc. IEEE/CVF Int. Conf. Comput. Vis.*, 2019, pp. 1273—1283.
- [36] Y. Chang, Z. Tu, W. Xie, B. Luo, S. Zhang, H. Sui, and J. Yuan, "Video anomaly detection with spatio-temporal dissociation," *Pattern Recognit.*, vol. 122, p. 108213, 2022.
- [37] S. Xingjian, Z. Chen, H. Wang, D.-Y. Yeung, W.-K. Wong, and W.-c. Woo, "Convolutional lstm network: A machine learning approach for precipitation nowcasting," in *Proc. 28th Int. Conf. Neural Inf. Process. Syst.*, 2015, pp. 802—810.
- [38] B. Ramachandra, M. J. Jones, and R. R. Vatsavai, "A survey of single-scene video anomaly detection," *IEEE Trans. Pattern Anal. Mach. Intell.*, vol. 44, no. 5, pp. 2293—2312, 2022.
- [39] K.-T. Nguyen, D.-T. Dinh, M. N. Do, and M.-T. Tran, "Anomaly Detection in Traffic Surveillance Videos with GAN-based Future Frame Prediction," in *Proc. Int. Conf. Multimedia Retrieval*. Association for Computing Machinery, 2020, pp. 457—463.
- [40] M. Mathieu, C. Couprie, and Y. Lecun, "Deep multi-scale video prediction beyond mean square error," in *Proc. Int. Conf. Learn. Representations*, 2016.
- [41] J. Kim and K. Grauman, "Observe locally, infer globally: a space-time mrf for detecting abnormal activities with incremental updates," in *Proc. IEEE Conf. Comput. Vis. Pattern Recognit.*, 2009, pp. 2921—2928.
- [42] J. T. Zhou, L. Zhang, Z. Fang, J. Du, X. Peng, and Y. Xiao, "Attention-driven loss for anomaly detection in video surveillance," *IEEE Trans. Circuits Syst. Video Technol.*, vol. 30, no. 12, pp. 4639—4647, 2020.
- [43] C. Lu, J. Shi, and J. Jia, "Abnormal event detection at 150 fps in matlab," in *Proc. IEEE Int. Conf. Comput. Vis.*, 2013, pp. 2720—2727.
- [44] D. P. Kingma and J. Ba, "Adam: A method for stochastic optimization," in *Proc. Int. Conf. Learn. Representations*, 2015.